AJNR

Detection of the Stellate and Thoracic Sympathetic Chain Ganglia with High-Resolution 3D-CISS MR Imaging

A. Chaudhry, A. Kamali, D.A. Herzka, K.C. Wang, J.A. Carrino and A.M. Blitz

AJNR Am J Neuroradiol published online 31 May 2018
http://www.ajnr.org/content/early/2018/05/31/ajnr.A5698

Published May 31, 2018 as 10.3174/ajnr.A5698

Detection of the Stellate and Thoracic Sympathetic Chain Ganglia with High-Resolution 3D-CISS MR Imaging

A. Chaudhry, A. Kamali, D.A. Herzka, K.C. Wang, J.A. Carrino, and A.M. Blitz

ABSTRACT

BACKGROUND AND PURPOSE: Despite the importance of the sympathetic nervous system in homeostasis and its putative role in various disease states, little is known regarding our ability to image the sympathetic chain and sympathetic chain ganglia, perhaps owing to their small size. In this retrospective study, we sought to evaluate the normal anatomy of the sympathetic chain ganglia and assess the detectability of the sympathetic chain and sympathetic chain ganglia on high-resolution 3D-CISS images.

MATERIALS AND METHODS: This study included 29 patients who underwent 3D-CISS MR imaging of the thoracic spine for reasons unrelated to abnormalities of the sympathetic nervous system. Patients with a prior spinal operation or visible spinal pathology were excluded. The sympathetic chain ganglia were evaluated using noncontrast 3D-CISS MR imaging. Statistical analyses included *t* tests and measures of central tendency. The Cohen κ statistic was calculated to evaluate interrater reliability.

RESULTS: The stellate ganglion and thoracic chain ganglia were identified in all subjects except at the T10–T11 and T11–T12 levels. The stellate ganglion was found inferomedial to the subclavian artery and anterior and inferior to the transverse process of C7 in all subjects. Thoracic sympathetic chain ganglia were identified ventral to the costovertebral junction in all subjects from T2 to T10. There was strong interobserver agreement for the detection of the sympathetic chain ganglia with $\kappa > 0.80$. The size, shape, and location of these structures corresponded with gross anatomic and surgical observations.

CONCLUSIONS: The thoracic sympathetic chain ganglia can be identified on precontrast 3D-CISS MR imaging. This technique may aid in the initial evaluation of stellate ganglion and/or sympathetic chain ganglia size and signal change for comparison in future studies.

ABBREVIATION: SCG = sympathetic chain ganglia

The autonomic nervous system is composed of a sympathetic component, responsible for the "fight or flight" response, and a parasympathetic portion, known for "rest and digest" functions. The sympathetic component differs in structure from the remainder of the peripheral nervous system. The sympathetic chain is generally divided into 2 nerve trunks that extend the entire length of the vertebral column along its lateral aspect.[1-3] The stellate ganglion provides sympathetic supply to the head, neck, and upper limbs, while the sympathetic chain ganglia (SCG) provide key innervations to the thoracic viscera, including the heart.[1-5] The stellate ganglion receives nerve fibers from the C6, C7, and T1 nerve roots with occasional contributions from T2, T3, and T4. The thoracic sympathetic chain receives nerve fibers from nuclei located within the lateral gray horn of the T2–T8 spinal segment that leave the spinal cord in the anterior rootlets of thoracic nerves, then traverse the white communicating rami, to enter the sympathetic trunk, synapsing onto their target postganglionic neurons in the paravertebral thoracic sympathetic ganglia. The postganglionic fibers traveling to the upper limb originate from the middle cervical ganglion, the stellate ganglion, and the upper thoracic ganglia; join the thoracic nerves through the gray rami communicantes; and then enter the brachial plexus and travel along different nerves to their end targets.[6,7]

Stellate ganglion and SCG blocks are performed for various conditions, including complex regional pain syndrome, postherpetic neuralgia, herpes zoster, causalgia, or intractable angina.[1] An SCG block can also be performed to treat patients with vaso-

Received March 19, 2017; accepted after revision April 19, 2018.

From the Departments of Neuroradiology (A.C., A.K.) and Radiology and Radiologic Sciences (A.M.B.), Johns Hopkins University School of Medicine, Baltimore, Maryland; Department of Biomedical Engineering (D.A.H.), Johns Hopkins University, Baltimore, Maryland; Department of Diagnostic Radiology and Nuclear Medicine (K.C.W.), University of Maryland, School of Medicine, Baltimore, Maryland; Imaging Service (K.C.W.), Baltimore VA Medical Center, Baltimore, Maryland; and Department of Radiology and Imaging (J.A.C.), Weill Cornell Medical College, Hospital for Special Surgery, New York, New York.

Please address correspondence to Ari M. Blitz, MD, Department of Radiology and Radiologic Sciences, Johns Hopkins University School of Medicine, 600 North Wolfe St, Phipps B-100, Baltimore, MD 21287; e-mail: ablitz1@jhmi.edu

http://dx.doi.org/10.3174/ajnr.A5698

spasm (eg, primary or secondary Raynaud phenomenon), phantom pain, cardiac arrhythmias (including long QT syndromes), and primary hyperhidrosis.[1-5] Patients are generally referred for SCG block due to persistence of symptoms (pain, vasospasm, hyperhidrosis, and so forth) despite medical management.[4,8-10] An SCG block is routinely performed in the clinical setting with sonography, fluoroscopy, or CT used to provide anatomic landmark guidance. However, the SCG itself is never directly visualized before the procedure.[10] Although the efficacy of interventions is well-established, a considerable proportion of patients do not see improvement and/or resolution of symptoms (eg, continued pain in up to 27.2%–33% in patients treated with SCG radiofrequency ablation for complex regional pain syndrome and recurrence of symptoms within 7 weeks in >66% of cases).[11] The reasons for the lack of short-term and long-term treatment benefit are not well-understood. Authors have suggested several possibilities, including incomplete SCG block secondary to anatomic variation.[2,11-14] In other words, it is possible that in some failed cases, the SCG was not directly and/or incompletely targeted because the structure itself was not actually visualized and was in a location variant from the commonly described one.

The peripheral components of the sympathetic nervous system have not been previously well-characterized on cross-sectional imaging, to our knowledge. There are only 2 small case series that identified the sympathetic chain ganglia on T1-weighted MR imaging,[2,12] primarily identifying the location of only the stellate ganglion.

The 3D-CISS refocused gradient-echo MR imaging sequence is a high-spatial-resolution technique performed to evaluate intracranial and spinal nerves.[15-20] 3D-CISS MR imaging generates images with contrast ideally proportional to the ratio of T2/T1 relaxation time, generating what appear to be heavily T2-weighted images.[18] In our experience, 3D-CISS MR imaging before intravenous contrast administration provides visualization in vivo of the sympathetic chain ganglia within the paravertebral fat. In this retrospective observational study, we aimed to evaluate the normal anatomy of the stellate ganglion and thoracic sympathetic chain ganglia and assess the detectability of each of the thoracic sympathetic chain ganglia on noncontrast CISS images.

MATERIALS AND METHODS

Study Group

This observational study was approved by the Johns Hopkins University institutional review board, and informed consent was waived in this Health Insurance Portability and Accountability Act–compliant retrospective study. Initially, 29 subjects underwent high-resolution CISS clinical MR imaging for the evaluation of either back pain or CSF leak. Subjects with other spine pathology, including 2 spinal tumors and 3 cases of prior spinal operations, were excluded from the study. Subjects were included in the study if the entire thoracic spine, including the thoracic inlet, was imaged. Studies were evaluated for image quality, and 1 scan with images degraded by motion artifacts was excluded. On the initial review of images, the SCG was noted to enhance uniformly on postcontrast images and became indistinct from surrounding tissue. Therefore, only precontrast CISS images were used to collect data on the SCG; 6 scans with only postcontrast images were excluded from the study for this reason. Only the first valid examination was included for each subject when multiple examinations had been performed. Ultimately, 24 examinations of 24 subjects were included for evaluation (Fig 1).

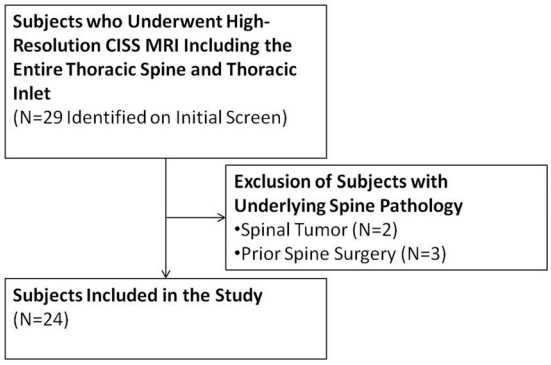

FIG 1. Flow diagram of included subjects. Of the 29 subjects screened, 24 were included in this study.

Imaging Protocol

The scans were obtained at 3T field strength with 0.6-mm isotropic image resolution. Typical imaging parameters were the following: TR/TE, 5.11/2.26 ms; 0.6-mm isotropic voxels; flip angle range, 25°–45°; FOV, 380 × 80 mm (read × phase encode); 320 × 80 acquisition matrix. Twenty-four subjects (10 men, 14 women) met the inclusion criteria.

Study Design

From the cohort of 24 patients who met the inclusion criteria, 480 normal thoracic sympathetic chain ganglia and 48 stellate ganglia were evaluated. Quantitative image analysis was performed by 2 independent readers blinded to each other's interpretation. The first reader, reader A, is a fellowship-trained radiologist with >6 years of experience. The second reader, reader B, is a first-year neuroradiology fellow. The detectability of the sympathetic chain ganglia was evaluated using precontrast enhanced 3D-CISS MR imaging. The expected location of the SCG was extrapolated from anatomy and surgical literature.[6,7] Both readers were credentialed neuroradiologists and had reviewed the anatomic literature before this study, to reach a consensus regarding the expected location of the sympathetic chain ganglia. A training or washout period was not attempted due to the limited number of subjects who met the inclusion criteria. The stellate ganglion is most commonly located anterior to the C7 vertebra transverse process, below the subclavian artery, superior to the first rib.[6,7] The thoracic SCG are located at the costovertebral junction anterior to the head of the ribs.[6,7] Confirmation of stellate ganglion and the SCG was made, ensuring connection of the SCG with spinal nerves and interconnection within the SCG chain on multiplanar (sagittal and coronal) reconstructions. The stellate ganglion is not entirely spheric or ellipsoid. Therefore, a calculation of volume using the largest diameter in each 3D plane would be misleading. Instead, the authors opted to quantify size consistent with reports in the anatomic literature.[6,7,21-26] The largest 2 axial dimensions of the ganglion were recorded (in millimeters), and surface area was subsequently obtained. Both readers were aware of the study objectives,

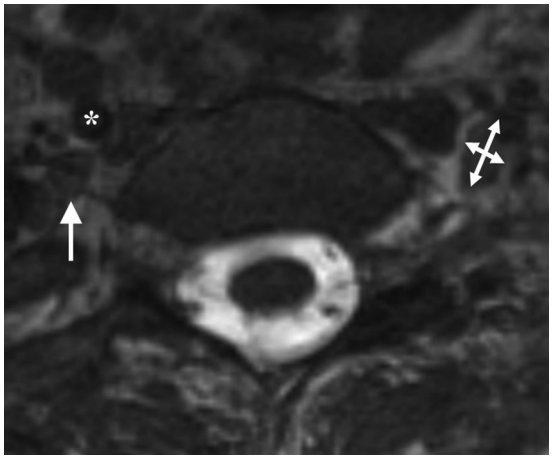

FIG 2. Axial oblique reformatted 3D-CISS MR imaging at C7 demonstrates the stellate ganglion (*arrow*) posterior to the subclavian artery (*asterisk*). The technique of measurement is demonstrated on the patient's left (*double-sided arrows*). The stellate ganglion was found inferior and anterior to the transverse process of C7 in all patients.

both reviewed the studies at different locations and times, and both were blinded to subjects' clinical data.

Statistical Analysis

Statistical analysis was performed using MedCalc for Windows, Version 12.5 (MedCalc Software, Mariakerke, Belgium). After controlling for subject sex, we performed measures of central tendency (mean, median) and a paired *t* test to assess differences between the mean sizes of the left and right SCG and to discern whether there was a difference in the observed size of the SCG between the right and left sympathetic chains. Additionally, a κ test was performed to evaluate interrater reliability.

RESULTS

In our cohort of 10 men and 14 women (mean age, 51.7 years), the stellate ganglion and thoracic chain ganglia were successfully identified in all subjects except at the T10–T11 and T11–T12 levels. The subjects enrolled in the study tolerated the MR imaging procedure well, and there were no acute complications during or immediately after this study.

Precontrast CISS demonstrated the stellate ganglion and SCG to be isointense relative to gray matter noted in the spinal cord. The stellate ganglion (Fig 2) and thoracic SCG (Figs 3 and 4) were present in all subjects in the expected location. The stellate ganglion (also referred to as T1 in anatomic texts[6]) was the largest of the sympathetic chain ganglia, with mean sizes of 36.62 ± 9.63 mm^2 on the right and 36.90 ± 8.9 mm^2 on the left. These size estimates were concordant with an anatomic study performed by Zhang et al.[7] The next 2 largest SCG were at T2 (13.70 ± 5.94 mm^2 on the right and 13.56 ± 5.25 mm^2 on left) and T3 (10.23 ± 2.85 mm^2 on the right and 10.21 ± 2.42 mm^2 on the left, Fig 3). The size of the SCG decreased in a craniocaudal direction from the stellate ganglia to the thoracolumbar junction (Fig 5). The T4- to T10-thoracic chain ganglia ranged from 4.1 to 19.35 mm^2. Table 1 summarizes the mean size and SD of the thoracic SCG. The 2-tailed *P* value demonstrated no significant difference between the mean values of the right and left sympathetic chain ganglia with a $P = .82$ (95% CI, −0.108 to 0.088). There was strong interobserver agreement for detection of the SCG with $\kappa > 0.8$.

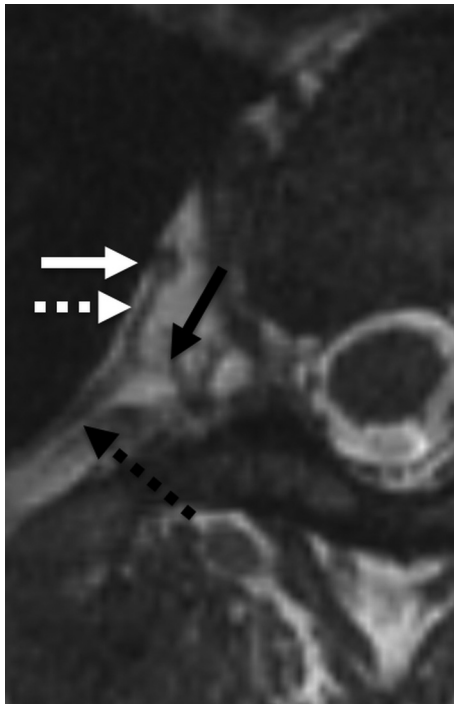

FIG 3. Axial oblique CISS MR imaging through the thoracic spine illustrates the sympathetic ganglion (*white arrow*), rami communicantes (*dashed white arrow*), and the ventral ramus (*black arrow*) and intercostal nerve (*dashed black arrow*).

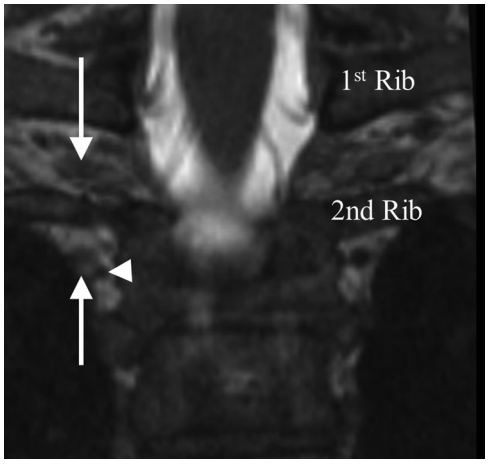

FIG 4. Coronal reformatted CISS through the upper thoracic region demonstrates the relationship of the second thoracic SCG (*down arrow*) with respect to the first and second ribs. The third SCG (*up arrow*) is seen just lateral to a venous flow void (*arrowhead*). The relationship of the SCG to adjacent venous structures is variable.

DISCUSSION

Isotropic or near-isotropic high-resolution 3D-CISS imaging provides the capability of visualizing structures not typically seen with standard spine MR imaging techniques. Our study shows that stellate and thoracic sympathetic chain ganglia can be readily characterized on precontrast 3D-CISS MR imaging. Our results demonstrate the stellate ganglia to be the largest of the SCG with a

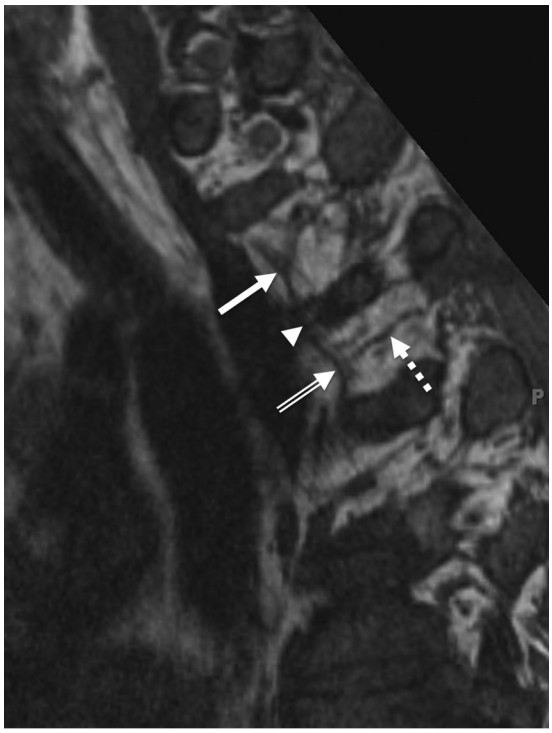

FIG 5. Sagittal oblique CISS through the paravertebral region oriented so that anterior is to the left of the image. The connection of the sympathetic chain ganglia (*solid* and *open arrows*) via the sympathetic chain (*arrowhead*) is visible. The rami communicantes (*dashed arrow*) are seen in continuity extending posteriorly toward the neural foramina.

Table 1: Summary of the mean size and SD of the thoracic SCG

SCG	Mean (mm^2)	SD (mm^2)
Stellate ganglion	36.76	9.27
T2	13.64	5.60
T3	10.22	2.64
T4	9.24	1.50
T5	8.80	1.07
T6	8.32	0.83
T7	8.05	0.75
T8	7.85	0.80
T9	7.60	0.84
T10	7.33	0.86

gradual decrease in size of the SCG at subsequent levels. Additionally, the stellate ganglia were noted to be the most lateral in location, with gradual medialization of the sympathetic chain trunk, with lower thoracic levels situated most medially. These findings are consistent with gross anatomic studies.[6,7,21-26] Prior studies have reported the size of the stellate ganglia, which vary ranging from 10 to 250 mm^2 (Table 2). The SCG size observed in our cohort, 35 mm^2, falls within the range reported by Hogan and Erickson,[3] Moore,[24] Kiray et al,[25] Zhang et al,[7] and Marcer et al.[26]

No prior systematic study identifies and characterizes the sympathetic chain ganglia using 3D-CISS technique. Two small case series previously reported by Hogan and Erickson[3] and Slappendel et al[12] have attempted to identify the stellate ganglion using MR imaging (with cohorts of 10 and 8 subjects, respectively). Both studies used T1-weighted imaging to demonstrate the stellate ganglion; however, these studies did not demonstrate the remainder of the thoracic sympathetic chain ganglia.

Table 2: Size of the stellate ganglion reported by prior studies

Author (Year of Publication)	Length (mm)	Width (mm)	Height (mm)
Anatomic/surgical specimen			
Moore (1954)[24]	25	10	5
Kiray et al (2005)[25]	20.6	8.3	3.9
Zhang et al (2009)[7]	19.3	6.3	
Marcer et al (2012)[26]	18.5	8.17	4.5
MRI-based measurement			
Hogan and Erickson (1992)[3]	10 (in largest dimension)		

Abnormalities of the SCG have been implicated in various conditions, including primary hyperhidrosis, reflex sympathetic dystrophy, Raynaud phenomenon, and so forth. Multiple interventional[1,2,4,5,8-14] and surgical[24-33] studies have reported resolution of clinical symptoms following SCG ablation, nerve block, or surgical resection of the sympathetic chain. However, none of these studies document pre- or postprocedure in vivo visualization of the SCG. The results of this pilot study show that 3D-CISS MR imaging is a safe and feasible technique that can reliably characterize the SCG. The knowledge derived from our study delineates the precise location of stellate ganglion and thoracic SCG.

There are several limitations of our study. This is a retrospective study and thus has disadvantages that are inherent to the design, including selection bias. Our cohort included only those patients who underwent high-resolution imaging for back pain or CSF leak, a population that may not be representative of the normally distributed population. Sample size is another limitation of the study, which may result in under- or overestimation of the mean size of the SCG at various levels. However, because our data appear to be congruent with the anatomic literature, the degree of variance between our results and the overall population may not be large. "Experimenter effect" is another potential limitation of this study. Because both readers were aware of the aim and design of this study, the measurement and final consensus of imaging characteristics could have been biased. Thus, our findings should be confirmed with a larger normally distributed patient cohort free of the aforementioned limitations.

CONCLUSIONS

The thoracic sympathetic chain ganglia can be readily seen and well-characterized on precontrast 3D-CISS MR imaging. This technique can aid in the initial evaluation of potential stellate and/or SCG pathology and allow posttreatment follow-up.

Disclosures: Kenneth Wang—*RELATED*: *Grant*: Radiological Society of North America, *Comments*: Fellowship Training Grant No. FT0904.* John Carrino—*UNRELATED*: *Board Membership*: Carestream Health, Halyard Health, GE Healthcare, *Comments*: medical advisory boards; *Consultancy*: Pfizer, Globus Medical, *Comments*: clinical trials. Ari Blitz—*UNRELATED*: *Consultancy*: Guerbet, *Comments*: medical-legal consulting and medical advisory; *Grants/Grants Pending*: R21 NS096497, U01DC013778, and grant for hydrocephalus research from Aesculap USA (Center Valley, PA).* *Money paid to the institution.

REFERENCES

1. Kim YU, Cheong Y, Kong YG, et al. **The prolongation of pulse transit time after a stellate ganglion block: an objective indicator of successful block.** *Pain Res Manag* 2015;20:305–08 CrossRef Medline
2. Elias M. **Cervical sympathetic and stellate ganglion blocks.** *Pain Physician* 2000;3:294–304 Medline
3. Hogan QH, Erickson SJ. **MR imaging of the stellate ganglion: nor-**

mal appearance. *AJR Am J Roentgenol* 1992;158:655–59 CrossRef Medline
4. Wong W. **Spinal nerve blocks.** In: Williams AL, Murtagh FR, eds. *Handbook of Diagnostic and Therapeutic Spine Procedures*. St Louis: Mosby; 2002:20–40
5. Erickson SJ, Hogan QH. **CT-guided injection of the stellate ganglion: description of technique and efficacy of sympathetic blockade.** *Radiology* 1993;188:707–09 CrossRef Medline
6. Kommuru H, Jothi S, Bapuji P, et al. **Thoracic part of sympathetic chain and its branching pattern variations in South Indian cadavers.** *J Clin Diagn Res* 2014;8:AC09–12 CrossRef Medline
7. Zhang B, Li Z, Yang X, et al. **Anatomic variations of the upper thoracic sympathetic chain.** *Clin Anat* 2009;22:595–600 CrossRef Medline
8. Shibata Y, Fujiwara Y, Komatsu T. **A new approach of ultrasound-guided stellate ganglion block.** *Anesth Analg* 2007;105:550–51 CrossRef Medline
9. Malmqvist EL, Bengtsson M, Sörensen J. **Efficacy of stellate ganglion block: a clinical study with bupivacaine.** *Reg Anesth* 1992;17:340–47 Medline
10. Feigl GC, Rosmarin W, Stelzl A, et al. **Comparison of different injectate volumes for stellate ganglion block: an anatomic and radiologic study.** *Reg Anesth Pain Med* 2007;32:203–08 Medline
11. Kastler A, Aubry S, Sailey N, et al. **CT-guided stellate ganglion blockade vs. radiofrequency neurolysis in the management of refractory type I complex regional pain syndrome of the upper limb.** *Eur Radiol* 2013;23:1316–22 CrossRef Medline
12. Slapppendel F, Thijssen H, Crul BJ, et al. **The stellate ganglion in magnetic resonance imaging: a quantification of anatomic variability.** *Anesthesiology* 1995;83:424–26 CrossRef Medline
13. Prithvi RP. **Stellate ganglion block.** In: Waldman SD, Steven D, eds. *Pain Management*. 2nd ed. Philadelphia: Saunders; 2011:1103–15
14. Price DD, Long S, Wilsey B, et al. **Analysis of peak magnitude and duration of analgesia produced by local anesthetics injected into sympathetic ganglia of complex regional pain syndrome patients.** *Clin J Pain* 1998;14:216–26 CrossRef Medline
15. Blitz AM, Choudhri AF, Chonka ZD, et al. **Anatomic considerations, nomenclature, and advanced cross-sectional imaging techniques for visualization of the cranial nerve segments by MR imaging.** *Neuroimaging Clin N Am* 2014;24:1–15 CrossRef Medline
16. Blitz AM, Macedo LL, Chonka ZD, et al. **High-resolution CISS MR imaging with and without contrast for evaluation of the upper cranial nerves: segmental anatomy and selected pathologic conditions of the cisternal through extraforaminal segments.** *Neuroimaging Clin N Am* 2014;24:17–34 CrossRef Medline
17. Soldatos T, Batra K, Blitz AM, et al. **Lower cranial nerves.** *Neuroimaging Clin N Am* 2014;24:35–47 CrossRef Medline
18. Yagi A, Sato N, Taketomi A, et al. **Normal cranial nerves in the cavernous sinuses: contrast-enhanced three dimensional constructive interference in the steady state MR imaging.** *AJNR Am J Neuroradiol* 2005;26:946–50 Medline
19. Yousry I, Moriggl B, Schmid UD, et al. **Trigeminal ganglion and its divisions: detailed anatomic MR imaging with contrast-enhanced 3D-constructive interferences in the steady state sequences.** *AJNR Am J Neuroradiol* 2005;26:1128–35 Medline
20. Sheth S, Branstetter BF 4th, Escottt EJ. **Appearance of normal cranial nerves on steady-state free precession MR images.** *Radiographics* 2009;29:1045–55 CrossRef Medline
21. Haam S, Kim D, Hwang J, et al. **An anatomical study of the relationship between the sympathetic trunk and intercostal veins of the third and fourth intercostal spaces during thoracoscopy.** *Clin Anat* 2010;23:702–06 CrossRef Medline
22. Singh B, Ramsaroop L, Partab P, et al. **Anatomical variations of the second thoracic ganglion.** *Surg Radiol Anat* 2005;27:119–22 Medline
23. Chung IH, Oh CS, Koh KS, et al. **Anatomic variations of the T2 nerve root (including nerve of Kuntz) and their implications for sympathectomy.** *J Thorac Cardiovasc Surg* 2002;123:498–501 CrossRef Medline
24. Moore DC. **Anatomy of the cervical and upper thoracic portions of the sympathetic nervous system.** In: *Stellate Ganglion Block: Techniques-Indications-Uses*. Springfield: Thomas; 1954:10–22
25. Kiray A, Arman C, Naderi S, et al. **Surgical anatomy of the cervical sympathetic trunk.** *Clin Anat* 2005;18:179–85 CrossRef Medline
26. Marcer N, Bergmann M, Klie A, et al. **An anatomical investigation of the cervicothoracic ganglion.** *Clin Anat* 2012;25:444–51 CrossRef Medline
27. Kim DH, Hong JY, Hwang JJ, et al. **Topographical considerations under video-scope guidance in the T2, T4 levels sympathetic surgery**. *Eur J Cardiothorac Surg* 2008;33:786–89 CrossRef Medline
28. Lin TS, Chou MC. **Treatment of palmary hyperhidrosis using needlescopic T2 sympathetic block by clipping: analysis of 102 cases.** *Int Surg* 2004;89:198–201 Medline
29. Inbar O, Leviel D, Shwartz I, et al. **Thoracic sympathectomy and cardiopulmonary responses to exercise.** *Eur J Appl Physiol* 2008;104:79–86 CrossRef Medline
30. Fiorelli A, D'Aponte A, Canonico R, et al. **T2–T2 sympathectomy versus sympathicotomy for essential palmary hyperhidrosis: comparison of effects on cardio-respiratory function.** *Eur J Cardiothoracic Surg* 2012;42:454–61 CrossRef Medline
31. Cerfolio RJ, De Campos JR, Bryant AS, et al. **The Society of Thoracic Surgeons expert consensus for surgical treatment of hyperhidrosis.** *Ann Thor Surg* 2011;91:1642–48 CrossRef Medline
32. Holland LC, Navaratnarakah M, Taggart DP. **Does surgical sympathectomy improve clinical outcomes in patients with refractory angina pectoris?** *Interact Cardiovasc Thorac Surg* 2016;22:488–92 CrossRef Medline
33. Coveliers H, Hoexum F, Rauwerda JA, et al. **Endoscopic thoracic sympathectomy for upper limb ischemia: a 16-year follow-up in a single center.** *Surgeon* 2016;14:265–69 CrossRef Medline